metals

MDPI

Article

Effect of Single-Pass DSR and Post-Annealing on the Static Recrystallization and Formability of Mg-Based Alloys

Christopher Hale *, Zhigang Xu *, Prithu Dhar, Svitlana Fialkova and Jagannathan Sankar

Center of Advanced Materials and Smart Structures (CAMSS), Department of Mechanical Engineering, North Carolina A&T State University, Greensboro, NC 27411, USA; pdhar1@aggies.ncat.edu (P.D.); sfialkov@ncat.edu (S.F.); sankar@ncat.edu (J.S.)

* Correspondence: clhale@ncat.edu (C.H.); zhigang@ncat.edu (Z.X.)

Abstract

Differential speed rolling (DSR) has been recognized as a unique processing technique in recent years, which has been used to plastically deform Mg-based alloys and to investigate the role of dynamic recrystallization (DRX) and its influence on both microstructure and mechanical properties. In this study, Mg–2Al–0.5Ca–0.5Mn (AXM20504) was solution-heat-treated (T4 condition) and subjected to single-pass DSR at both 20 and 40% thickness reductions, followed by post-annealing at temperatures of 350, 400, and 450 °C for the durations of 20, 40, and 60 min to evaluate the onset and development of static recrystallization (SRX) and its overall effect on the formability of Mg-based alloys. The results demonstrate how post-annealing yields nearly complete SRX at 400 °C for 60 min and 450 °C for 40 min with a significant improvement in ductility, increasing from 5% to 12% while maintaining an average tensile strength above 200 MPa. Thus, the improvement in mechanical properties demonstrates that post-annealing can deliver significant potential in terms of the enhanced formability of Mg alloys used in sheet metal forming applications.

Keywords: magnesium alloys; differential speed rolling (DSR); post-annealing; dynamic recrystallization (DRX); static recrystallization (SRX); grain refinement

1. Introduction

Magnesium and its alloys are increasingly important in structural and automotive industries, due to their lightweight nature, which contributes to an improved fuel economy and reduced exhaust emissions [1]. However, their broader application is limited by poor formability at room temperature, which is primarily due to their hexagonal close-packed (HCP) crystal structure [2]. Grain refinement and texture modification have shown promise as effective strategies to enhance room-temperature formability [3]. Additionally, using thermally activated processes such as post-annealing to achieve static recrystallization offers a practical means of controlling grain structure and crystallographic texture. These processes help to soften the material to restore its ductility and formability after deformation.

Most research on magnesium alloys has focused on dynamic recrystallization following mechanical deformation [4–7], which includes processing techniques such as conventional and differential speed rolling in various types of Mg alloys [8,9], while comparatively less attention has been given to static recrystallization [10–12]. This is primarily due to the limited deformability of magnesium alloys at low temperatures. However, recent efforts—such as alloying additions and modifications to strain paths—have aimed to enhance ductility and broaden the processing window, utilizing in situ studies to observe

Check for updates

Academic Editor: Dmitri Molodov

Received: 7 November 2025
Revised: 17 December 2025
Accepted: 18 December 2025
Published: 1 January 2026

Copyright: © 2026 by the authors. Licensee MDPI, Basel, Switzerland. This article is an open access article distributed under the terms and conditions of the Creative Commons Attribution (CC BY) license.

the process in real time and computational models to predict its behavior under various conditions [13–15]. As a result, there is growing interest in understanding the role of recovery in recrystallization behavior, the evolution of microstructure and texture during recrystallization, and the mechanisms of grain coarsening in magnesium alloys.

Static recrystallization is a thermally activated process in which new, strain-free grains nucleate and grow, replacing the deformed microstructure through the formation and migration of high-angle grain boundaries (HAGBs). As previously noted, magnesium alloys often exhibit incomplete recrystallization and a strong retention of deformation texture—specifically, the basal texture (0001) after the rolling process [10,11,16]. This retained texture is detrimental to sheet formability and significantly limits the widespread use of magnesium alloys in structural applications. Several factors contribute to the persistence of the deformation texture after annealing. These include a limited number of nucleation sites that are capable of generating grains with non-basal orientations, incomplete recrystallization across large regions of the material, and the restricted ability of the grain boundaries to undergo bulging [10–12]. Collectively, these factors hinder texture weakening during dynamic recrystallization, posing a major challenge in the processing of magnesium alloys.

Plastic deformation in magnesium occurs through the activation of various slip and twinning systems. Among these, basal slip is the easiest mode of deformation, with a relatively low critical resolved shear stress (CRSS) of approximately 0.5 MPa. As reported by Barnett, the CRSS ratio for basal <a> slip, {101–2} extension twinning, prismatic <a> slip, and pyramidal <c + a> slip is 1:0.7:2:15 [17]. In addition to basal slip, non-basal slip systems—including prismatic <a>, pyramidal <a>, and pyramidal <c + a>—can also be activated. However, these systems require significantly higher CRSS values to initiate slip. For instance, the CRSS for prismatic slip is around 44 MPa, while pyramidal slip systems require approximately 40 MPa [18]. This large difference in CRSS makes non-basal slip difficult to activate under typical deformation conditions, thereby contributing to the basal texture and the limited ductility of magnesium alloys, especially at room temperature. Improvement in ductility has been accomplished through post-annealing, which has been shown to assist in the activation of non-basal slip—including prismatic slip [18].

Other studies have emphasized the importance of the rolling temperature in the microstructural development of Mg-based alloys like AZ31 to produce a more homogenous and fully recrystallized microstructure, which has been in the range of 350 °C [19,20]. Usually, the uniform fine microstructure produced by DSR, along with the corresponding high strength, are the result of cross-shear deformation [21,22]. While higher rolling temperatures have improved the elongation to failure, they also result in some decrease in both yield strength (YS) and ultimate tensile strength (UTS) [19].

In the previous study, the materials under investigation consisted of Mg-*x*Al-*y*Ca-*z*Mn (AXM) alloys with a fixed amount of Al and Mn (both 0.5 wt%) and varying amounts of Ca (from 0.15 to 1.5 wt%) subjected to single-pass DSR to analyze the effect on DRX, as well as the effect on the microstructure and mechanical properties [23]. This study, along with various other studies, has shown the development of high-strength Mg-*x*Al-*y*Ca-*z*Mn alloys with higher Ca/Al ratios—but often with a sacrifice to ductility [7,24]. Based on analyses in the previous work, the composition of Mg-2Al-0.5Ca-0.5Mn was used in this study for the evaluation of post-annealing and its influence on SRX [23]. Furthermore, to achieve a balance in strength and ductility, post-annealing was performed to investigate its impact on ductility, tensile strength, and the formability of the alloy.

With special consideration to the importance of DSR and post-annealing, this paper aims to address the relationship between the microstructure and mechanical properties of Mg-based alloys, specifically AXM alloys, to provide a deeper understanding of the SRX process and influence on formability. This knowledge contributes to a greater understand-

ing of the performance of Mg-based alloys and methods to optimize both fabrication and forming, which is useful in large-scale production applications. While strength has been shown to be significantly improved through DSR, the elongation-at-break (and corresponding ductility) has been diminished. In this paper, a significant improvement in ductility while maintaining tensile strength has been shown through post-annealing, where the new grains (growth of DRX grains) are developed through static recrystallization, thereby diminishing the limitations of the basal texture and improving the ductility and formability of the Mg alloy.

2. Materials and Methods

2.1. Materials Preparation

As in our previous work with AXM alloys, the casting process used a box-melting furnace and a preheated permanent steel mold in an argon-filled glove box [23]. PANDAT software Version 2020 (Middleton, WI 53562, USA) was used to determine the composition [25]. Based on a previous study, Mg-2Al-0.5Ca-0.5Mn (also referred to as AXM20504) was the chosen composition for the ingot prepared for the rolling and post-annealing evaluation [23]. After a T4 heat treatment at 500 °C for 30 h, the T4-treated alloy ingot with a size of 28 mm × 28 mm × 104 mm was cut into rectangular plates with dimensions of 65 mm long, 24 mm wide, and a thickness of 4 mm by wire EDM (Sodick VL400Q, Schaumburg, IL, USA) and prepared for differential speed rolling.

2.2. Rolling

The plates cut by wire EDM were chamfered on each edge to reduce the potential for side cracking and labeled for rolling at 20% reduction and 40% reduction, for comparison at a lower reduction to a higher reduction—similarly to reductions chosen in previous work [23]. These reductions were chosen to represent an earlier onset of DRX and SRX at 20% to more complete DRX and SRX at a higher reduction of 40%. The mill speed was set to 4 m/min for the top and 2 m/min for the bottom rolls, and boron nitride lubricant was applied to the surface of the rolls prior to rolling to prevent the material from sticking to the surface of the rolls. Also, the roll temperature was maintained at 300 °C.

2.3. Post-Annealing

Post-annealing on the 20% and 40% rolled AXM samples was performed in a furnace, using the matrix of duration and temperatures. The temperatures of 350, 400, and 450 °C for durations of 20, 40, and 60 min were used for post-annealing, since previous studies have shown this regime to be the most effective in the SRX process [23,26]. Samples were then removed from the furnace and quenched in water to retain the microstructure.

2.4. Microstructural Characterization

Both the as-rolled and post-annealed AXM alloys were prepared for SEM/EBSD metallography using standard mechanical grinding SiC papers and final polishing, using 0.05 µm Al_2O_3 suspension to the mid-section of the sample thickness. Subsequently, the samples were etched with a mixture of 10% nitric acid and picric acid to highlight grain boundaries for optical microscopy. The AXM sample specimens were subjected to ion milling (Fischione Instruments, Model 1061, Export, PA, USA) to prepare for scanning electron microscopy (SEM) and electron backscatter diffraction (EBSD). Ion milling was performed for 2 h at 4 kV, followed by another 2 h at 2 kV, with 2° tilt for both steps. For the AXM alloys, microstructural features were examined on the normal direction (ND) plane. Chemical composition was analyzed using energy-dispersive X-ray spectroscopy (EDS),

and crystallographic information was obtained via EBSD (Symmetry, Oxford Instruments, Abingdon, UK), integrated with an SEM (SU8000, Hitachi, Chiyoda City, Tokyo, Japan).

The crystallographic information acquired by EBSD allowed for the generation of inverse pole figure (IPF) maps and pole figures, facilitating the examination of the quantity and grain size of dynamically recrystallized (DRX) grains and the pole figure intensity and orientation of the grains. Images were captured at various magnifications, including 50×, 200×, 500×, and 1000×, for close examination of microstructural features taken from the mid-region of the DSR processed sample. The EBSD scanning utilized the acquisition parameters of 15 kV and 15 µA. Aztec Version 6.0 and Aztec Crystal Version 2.2 software played a vital role in conducting various measurements and analyses, including DRX grain measurements, area fraction measurements, pole figures, tilt angles, and low/high grain-boundary angles. The integration of EBSD and associated software contributed to a comprehensive understanding of the microstructural characteristics, offering insights into the amount, size, and distribution of DRXed grains and the orientation of grains and associated pole intensity.

2.5. Mechanical Testing

Three tensile specimens were prepared according to ASTM E8/ASTM E8M [27], using a wire-EDM for the T4, as rolled, and the annealed samples. The cutting direction of the tensile specimens was parallel to the rolling direction. Dimensions at the gauge were 15 mm in length, 3.0 mm in width, and 3.2 mm thick for the 20% reduction, and 2.4 mm thick for the 40% reduction plates. All the samples were tested using the Instron Model 3000 machine (Instron, Norwood, MA, USA) at an estimated strain rate of 1.1×10^{-3} s^{-1}.

3. Results

3.1. Microstructure of the Alloys

3.1.1. Microstructure Evolution of DSR Samples

IPF maps for the AXM-rolled samples (DSR 4:2 at 400 °C) in Figure 1 show a thickness reduction at (a) 10%, (b) 20%, (c) 30%, and (d) 40% with a magnification of 500× where the development of DRX grains is shown. The IPF maps demonstrate that few DRX grains present at 10% (as similar to the original solution treated T4) and an increasing number of DRX grains present at 40%. The average grain size at 10% reduction was 31.9 ± 28.2 µm, decreasing to 19.5 ± 14.2 µm at 40% reduction, with the DRX area fraction doubling from 10 to 40% reduction following DSR [23,26]. An inset band contrast image showing the fine DRX grains is provided in Figure 1d. The associated pole figures are also positioned in the corners, showing the basal texture increased as the thickness reduction increased.

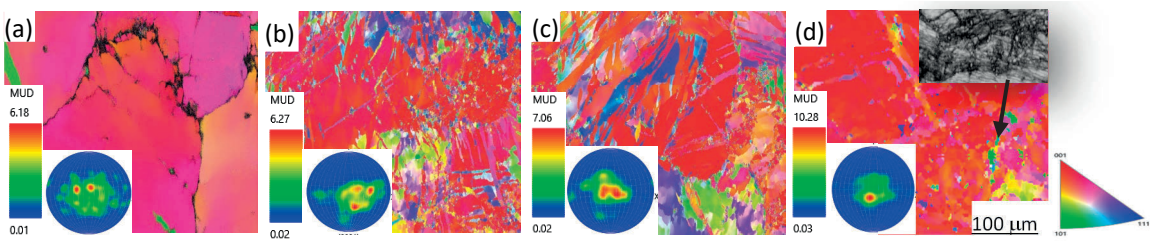


Figure 1. IPF maps for the as-rolled AXM20504 alloys following DSR 4:2 at 400 °C , with the thickness reductions of (**a**) 10% (**b**) 20%, (**c**) 30%, and (**d**) 40%, as well as the insets of the pole figures for each condition that are generated from the scans.

The XRD scan comparing the original solution-treated (T4) condition to the DSR at 40% can be seen in Figure 2. The scan shows that the T4 shows 97% magnesium phase with only trace amounts (less than 3%) of secondary phases. In comparison, the DSR at

40% reduction shows 6% of secondary phases, with Al-Mn also being one of the main secondary phase constituents after rolling. Also, the intensity of the (0002) peak did increase for the rolled material, as compared to the T4 initial condition due to the strengthening of the basal texture after rolling, and this is consistent with EBSD data.

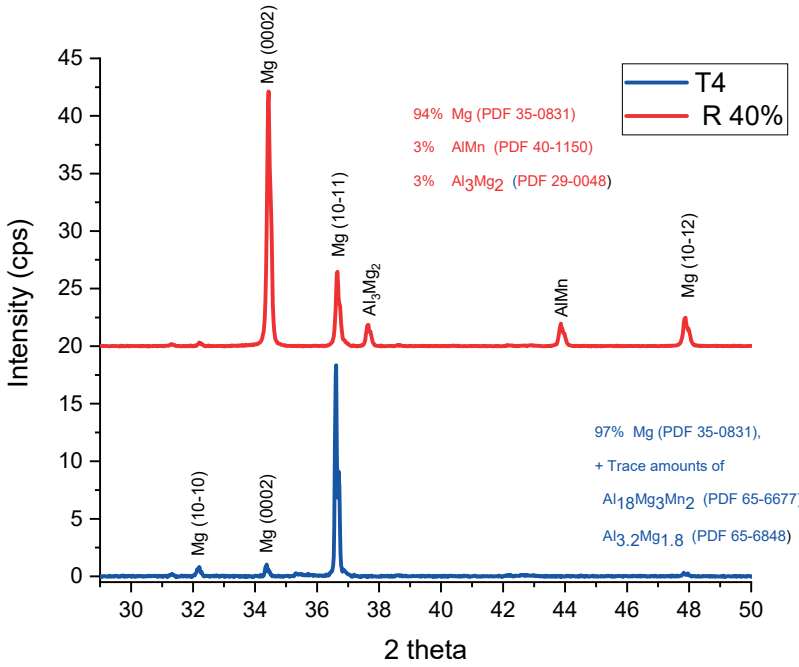


Figure 2. XRD scans for original solution, heat treated (T4) as compared to the as-rolled AXM20504 at 40% DSR 4:2, showing comparison of the phases present.

3.1.2. Microstructure Evolution of Post-Annealed Samples

In Figure 2, the comparison of T4 to DSR at 40% reduction is shown to identify the phases that are present. In an evaluation of the DSR processed and post-annealed specimens through EBSD, the Al-Mn and Al-Mg secondary phases were present at similar percentages. The presence of these phases has also been shown and discussed in previous studies, but it is not the primary focus of this paper [23,26].

In Figure 3, the post-annealed AXM20504 that was rolled at 20% thickness reduction demonstrates the effect on the microstructure and the development of the SRX process over various temperatures and durations. In Figure 3a–c, the annealing temperature was 350 °C and shows an increase in grain size of those formed by SRX from (a) 20 min to (b) 40 min and (c) 60 min. However, the percent SRX at 60 min was only 68% at 350 °C. This demonstrates that the temperature was not high enough to complete the SRX process. In Figure 3d–f, the annealing temperature was 400 °C and it shows an increase in grain size as well as normalizing of the grain size—with almost complete static recrystallization at 91%, as seen in (f), at 400 °C for 60 min. In Figure 3g–i, the annealing temperature is 450 °C and significant SRX occurs at (g) 20 min with almost full SRX (99%) achieved at (h) 450 °C for 40 min. Over grain growth is shown at 450 °C for 60 min.

Figure 4 shows the pole figures for the annealed alloys, where there was a spreading of the pole even at 20% reduction, as compared to the DSR 20% alloy prior to annealing, as well as decreased pole intensity with most post-annealing samples being below a maximum intensity of 6, as compared to maximum intensity of 9 or 10 for the as-rolled specimens prior to annealing. This spreading of the pole also indicates a weakening of the basal texture for the post-annealed alloys, where the texture spreads out further from the center of the pole figure. In the as-rolled alloys, the basal texture is stronger and contained closer to the center, with a much higher intensity. Thus, many of the deformed grains have a much more

heavily defined basal texture that is weakened after annealing, as seen in the majority of the pole figures in Figure 4. Also, the pole intensity shows a general decreasing trend with an increase in annealing time, which demonstrates a weakening of the basal texture. Likewise, an increase in post-annealing temperature from 350 to 450 °C exhibits a general decreasing trend in pole intensity, also demonstrating a weakening of the basal texture.

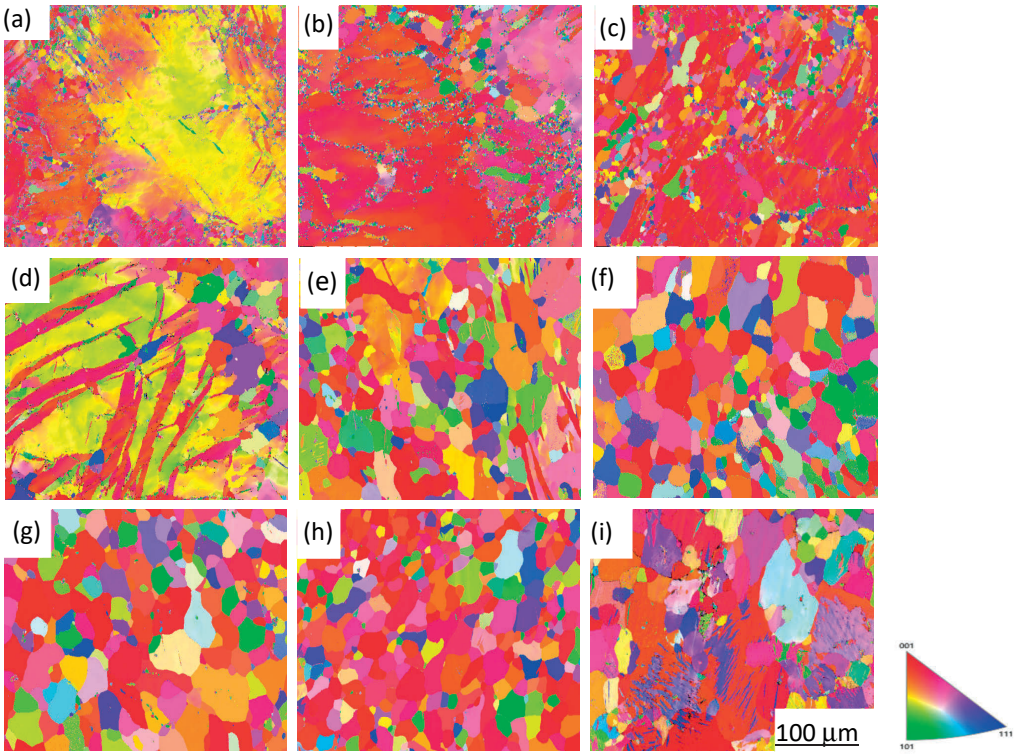


Figure 3. IPF maps showing the grain refinement evolution for AXM20504 (DSR 4:2 m/min at 400 °C and 20% reduction) after post-annealing with the combination of temperatures and durations at 350 °C, for (**a**) 20 min, (**b**) 40 min, and (**c**) 60 min; at 400 °C, for (**d**) 20 min, (**e**) 40 min, and (**f**) 60 min; and at 450 °C, for (**g**) 20 min, (**h**) 40 min, and (**i**) 60 min, respectively.

The average grain sizes for the AXM20504 for the post-annealed samples at given durations and temperatures are shown in Figure 5. The original grain size (T4) is 60 µm, which is reduced to 35 µm at a DSR 20% reduction. There is a marginal difference in grain size for the annealed conditions but a slight reduction in grain size for the higher temperature at 450 °C, demonstrating that the recrystallization process aided in normalizing and generating a more uniform grain size.

Figure 5 shows the IPF maps for the annealed AXM20504 that was rolled at 40% reduction. Again, the crystallization (SRX) is observed with increasing time (seen at 350 °C as well as 400 °C). However, SRX is observed as being nearly complete, going from 20 to 40 min for 450 °C, where grains are more similar in size with almost no parent grains left and mostly recrystallized grains are present, as quantified in Figure 6.

In Figure 7, the pole figures are shown for the annealed alloys, where there was a spreading of the pole at 40% reduction, as compared to the as-rolled DSR 40% alloy, as well as an overall decreased pole intensity, with most being below a maximum of eight or nine, as compared to higher pole intensities for the as-rolled alloys. As has been shown in the literature, a spreading of the poles indicates an improvement and weakening of the basal texture, which also tends to improve ductility [27,28]. With an increase in time for each of the temperatures, the pole is observed to spread outward in the pole figure and a slight tilt away from the center is also observed. As seen in the pole figures for the 20% reductions, the pole intensity for 40% also shows a general decreasing trend with

the increase in annealing time, which also demonstrates a weakening of the basal texture. Likewise, an increase in the post-annealing temperature exhibits a general decreasing trend in pole intensity, which is also associated with a weakening of the basal texture.

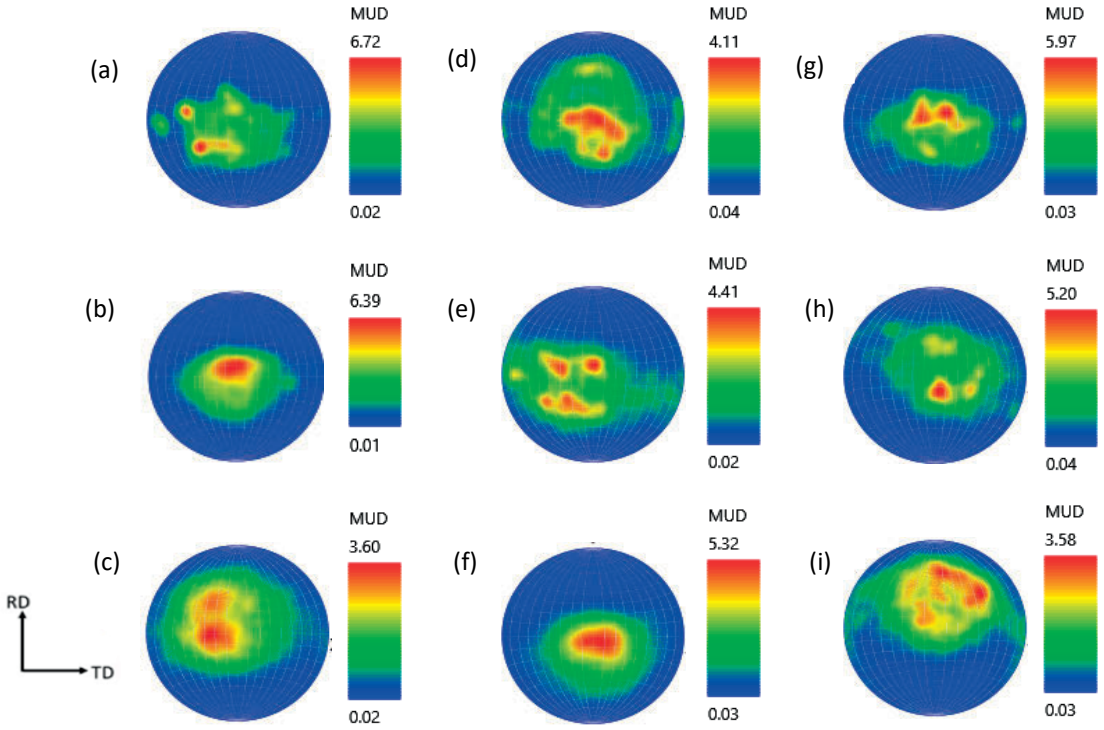


Figure 4. Pole figures for AXM20504 (DSR 4:2 m/min and 20% reduction) after post-annealing, showing the orientation spreading and evolution (scan taken at 50×) at 350 °C for (**a**) 20 min, (**b**) 40 min, (**c**) 60 min; 400 °C for (**d**) 20 min, (**e**) 40 min, and (**f**) 60 min; and at 450 °C for (**g**) 20 min, (**h**) 40 min, and (**i**) 60 min.

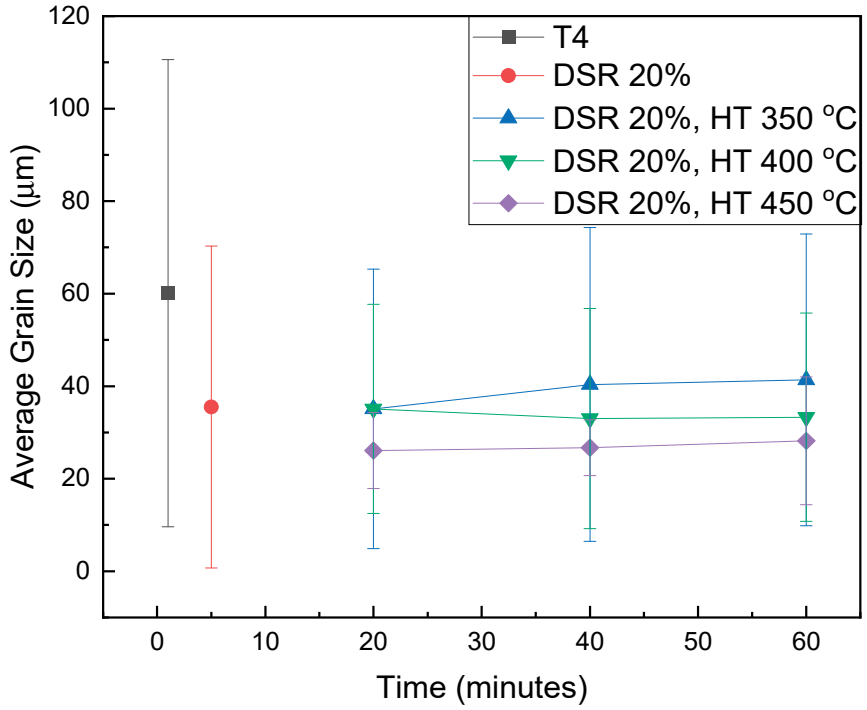


Figure 5. Average grain size of AXM20504 (DSR 4:2 m/min and 20% reduction) after post-annealing.

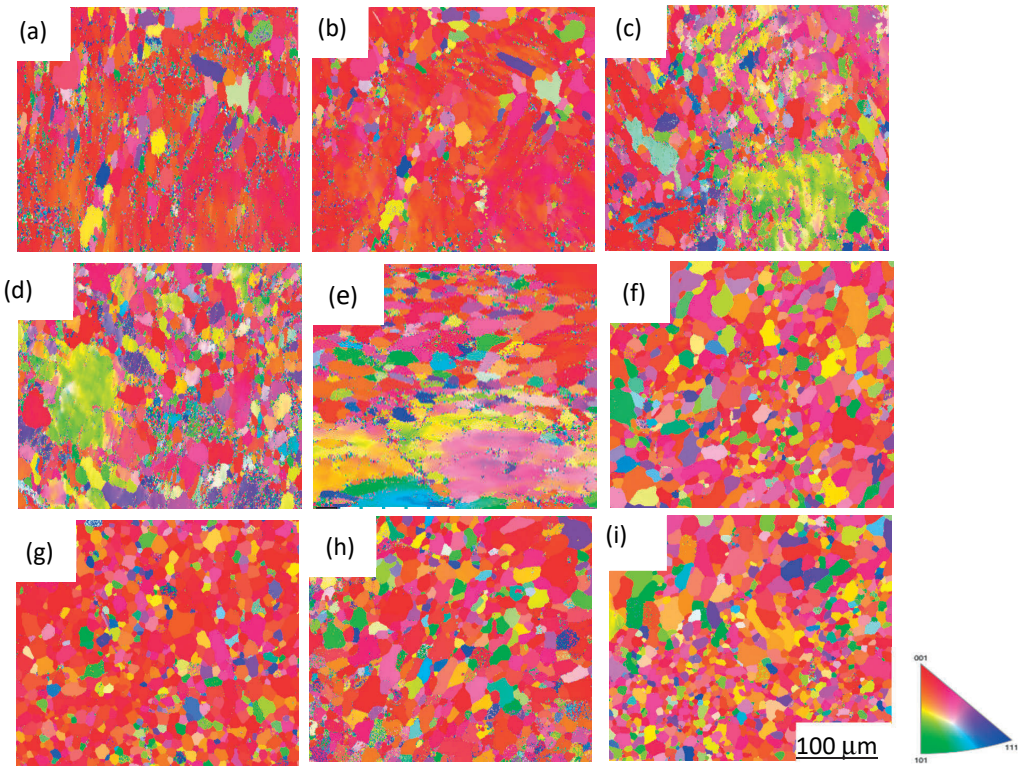


Figure 6. IPF maps for AXM20504 (DSR 4:2 m/min at 400 °C and 40% reduction) after post-annealing, showing the grain refinement evolution at 350 °C for (**a**) 20 min, (**b**) 40 min, (**c**) 60 min; at 400 °C for (**d**) 20 min, (**e**) 40 min, and (**f**) 60 min; and at 450 °C for (**g**) 20 min, (**h**) 40 min, and (**i**) 60 min.

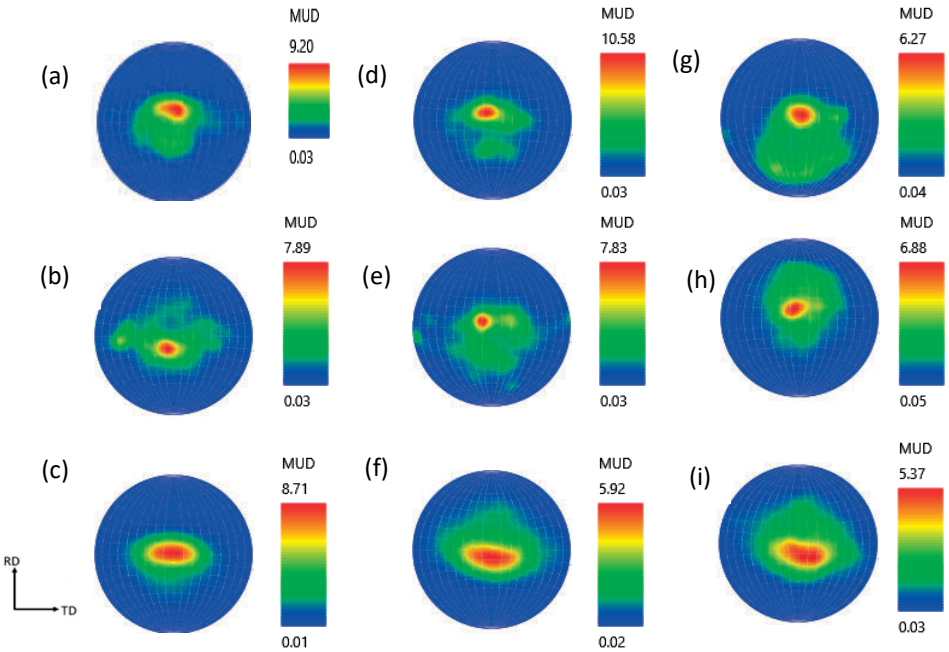


Figure 7. Pole figures for AXM20504 (DSR 4:2 m/min and 40% reduction) after post-annealing, showing the pole figure spreading and evolution at magnification of 50x at 350 °C for (**a**) 20 min, (**b**) 40 min, (**c**) 60 min; at 400 °C for (**d**) 20 min, (**e**) 40 min, and (**f**) 60 min; and at 450 °C for (**g**) 20 min, (**h**) 40 min, and (**i**) 60 min.

Figure 8 shows the average grain size for the AXM20504 for the given temperature and duration, calculated using AztecCrystal Version 2.2. As previously stated, there is a slight decrease in grain size at 450 °C for 20, 40, and 60 min, showing how the grain size

becomes more uniform with less deviation during the static recrystallization process. The increasing development of new grain boundary area from post-annealing can subsequently explain the increase in ductility at 20% and 40% reduction, where slip can more easily occur on all the newly formed grain boundaries and within the grains as part of the SRX process. There is also a general trend observed in grain growth, with increasing time for each temperature. Also, the figure shows that the grain size of the annealed alloys is only slightly larger, as compared to the DSR at 40%, but it still remains significantly less than the original T4 condition.

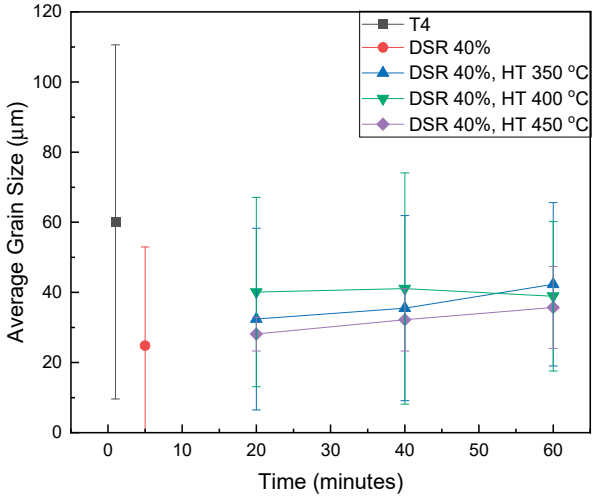


Figure 8. Average grain size of AXM20504 (DSR 4:2 m/min and 40% reduction) after post-annealing at 350 °C, 400 °C, and 450 °C.

In Figure 9, the area fraction of SRX for the AXM20504 alloy after post-annealing is shown as a function of temperature and duration. The figure shows that the most complete SRX occurred for the DSR; 20% and 40% were post-annealed at the highest temperature of 450 °C, particularly at a duration of 40 min. The higher temperature shows a more complete process of relieving internal stresses developed through plastic deformation during DSR, and a higher degree of recrystallization achieved in the formation of new grains.

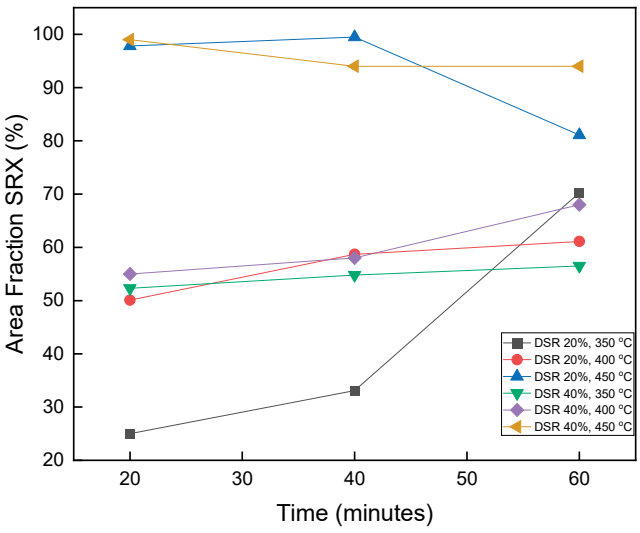


Figure 9. Area fraction of SRX for AXM20504 after post-annealing, showing the effect of temperature and duration on SRX for both DSR 20% and 40% specimens.

3.2. Mechanical Properties

3.2.1. Relationship of Hardness and Post-Annealing Temperature/Duration

The relationship between hardness and post-annealing temperature/duration are shown in Figure 10 for DSR with a rolling speed of 4:2 m/min at both 20% and 40% reductions. The figure shows that the hardness is highest for the material annealed at 350 °C and also shows a downward trend with an increase in time. Also, it shows that all hardness of post-annealed specimens is significantly less than the rolled DSR 4:2 at 40%, which is expected. The hardness of the original solution-heat-treated condition (T4), however, is not much different than the annealed samples.

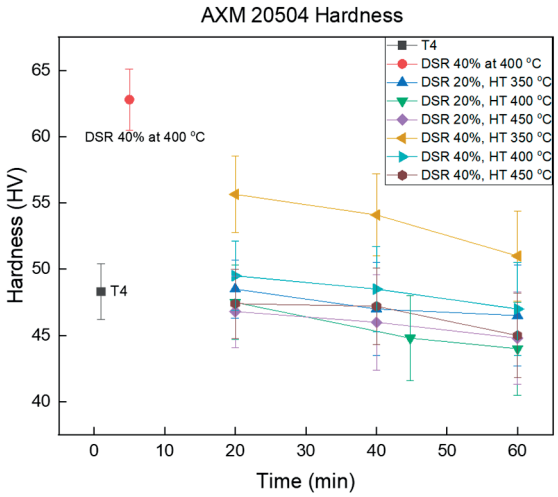
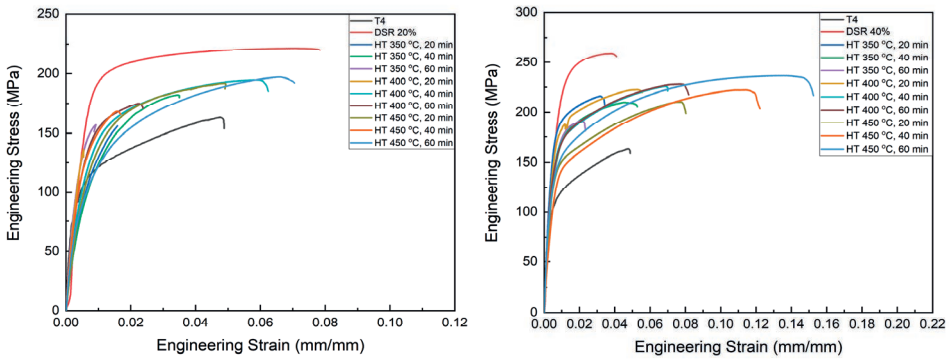


Figure 10. Hardness for T4, DSR 20% and 40% at 400 °C, as well as the post-annealed temperatures of 350, 400 and 450 °C for different durations of 20,40 and 60 min.

3.2.2. Tensile Behavior of Post-Annealed Samples

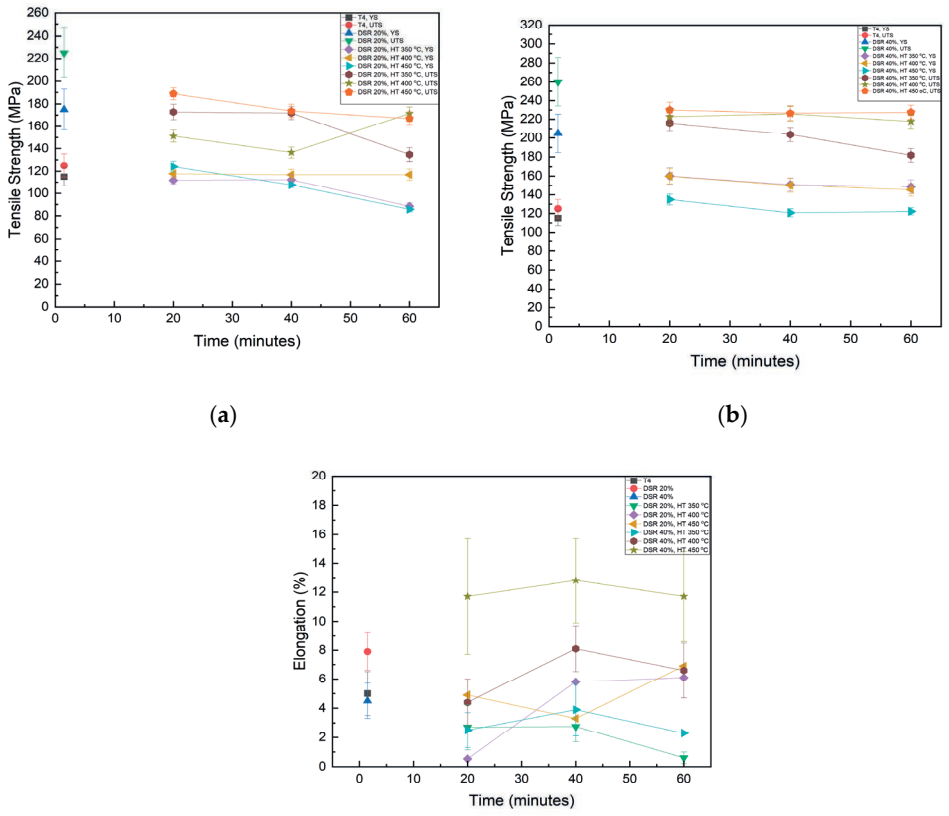
The tensile stress–strain curves for the DSR 20% at 4:2 m/min that were post-annealed samples can be seen in Figure 11a, while those for the DSR 40% post-annealed samples can be seen in Figure 11b. The maximum elongation-at-break for the post-annealed with 20% DSR reduction was approximately 7 ± 3.4% and the maximum strength was 198 ± 6.2 MPa for the material annealed at 450 °C for 60 min. However, the elongation at the break was much higher for the DSR 40% annealed at 450 °C and 40 min, reaching 12 ± 3.5%. The original as-rolled DSR 20% and 40% both had higher ultimate tensile strengths of 225.0 ± 15.2 MPa and 260.0 ± 25.8 MPa, respectively, with elongations of breaks of 7.9 ± 3.2% and 4.5 ± 1.5%, respectively. The effect of post-annealing demonstrates a significant improvement in ductility for DSR at 40%, as compared to the as-rolled specimen. While there was a drop in tensile strength for the DSR 40% with post-annealing, most of the post-annealed samples maintained a tensile strength above 200 MPa.

The strength and ductility of AXM20504, comparing the original T4 solution-treated state to the processed DSR at 20% and 40% and post-annealed, are presented in Figure 12. The figure shows the comparison after annealing for the specified temperature and duration. The post-annealed samples show the best ductility and the corresponding tensile strength for higher temperatures (i.e., 400 and 450 °C), while maintaining a relatively high strength, above 200 MPa, and ductility with elongation around 12% for 450 °C. In comparison, the as-rolled DSR at 20% had an ultimate tensile strength of 225.0 ± 15.2 MPa and the 40% had an average tensile strength of 260.0 ± 25.8 MPa [23]. Thus, significant improvement in both the ultimate tensile strength and ductility was achieved after DSR processing combined with post-annealing.



(**a**) (**b**)

Figure 11. Stress–strain curves for AXM20504 (DSR 4:2 m/min), showing comparison of T4, DSR, and after post-annealing for (**a**) DSR 20% and (**b**) DSR 40%.



(**a**) (**b**)

(**c**)

Figure 12. Comparison of T4 to (**a**) DSR at 20% with post-annealing and (**b**) DSR at 40% with post-annealing, as well as (**c**) % elongation to failure.

4. Discussion

One of the goals of this study was to improve ductility while retaining strength, which would also aid in the formability of the alloys. According to the Hall–Petch theory, a material's hardness and strength increases as its grain size decreases, or vice versa. As seen in Figure 10, the hardness effectively decreased as the post-annealing increased the grain size. Furthermore, previous work showed differential speed rolling, which resulted in improved tensile strength but decreased ductility [23]. Post-annealing of the AXM alloy was essential to improving ductility by weakening the basal structure, which was accomplished through static recrystallization. Post-annealing of the alloy demonstrated nearly complete static recrystallization, as seen in Figure 9. As seen in Figure 12b, the improvement in

ductility was particularly seen at temperatures of 400 and 450 °C for DSR 40%, wherein the higher temperatures were able to provide the energy needed to activate the SRX process and also relieve internal stresses produced from DSR. The internal stress is a function of dislocation density and can be expressed through the kernel average misorientation (KAM). KAM analysis for the post-annealed DSR 40% alloys can be seen in Figure 13. In the figure, the KAM number is significantly less at 450 °C compared to both temperatures at 350 and 400 °C. A high KAM value indicates a high degree of local lattice distortion and suggests that a material has undergone significant plastic deformation, which creates a high density of geometrically necessary dislocations. A low KAM, on the other hand, indicates a small degree of local lattice distortion, which is observed when a material has undergone less plastic deformation or has been annealed to relieve the internal stresses.

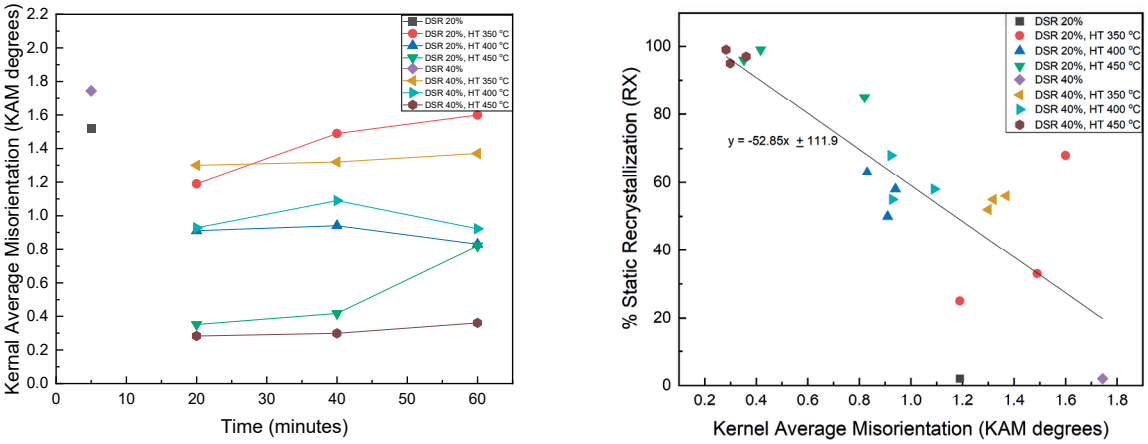


Figure 13. Influence of post-annealing temperature and duration on the kernel average misorientation (KAM degrees) for DSR 20% and 40% at 350, 400, and 450 °C.

Post-annealing of the alloys resulted in an improvement in ductility; however, it did not significantly reduce tensile strength compared to the DSR 20% and 40%, as seen in Figure 11. The average tensile strength of the DSR 40% as rolled was 220 MPa, compared to the average strength of post-annealed alloys, which was above 200 MPa [23]. Thus, the ductility and overall formability of the Mg alloys were improved through the post-annealing process with the relieving of internal stresses (created through the DSR process) that allowed easier activation of slip along the prismatic and basal planes. The formability of the alloys is evaluated by their strain-hardening properties, as well as the uniform elongation before necking (the localized reduction in the cross-sectional area). The strain-hardening exponent (n-value) quantifies a metal's ability to become stronger through plastic deformation, with higher values indicating greater hardening and better formability. The uniform elongation represents the maximum strain a material can sustain while deforming uniformly. A higher n-value and a higher uniform elongation will allow for the material to be formed into more complex shapes before necking occurs. The n-value is determined by using the true-stress and true-strain curve and using the Hollomon equation ($\sigma = K\varepsilon^n$), where K is the strengthening coefficient, n is the strain-hardening exponent, σ is the true stress, and ε is the true strain [29]. For Mg alloys, the range of the strain-hardening exponent (n) can vary but typically falls between 0.1 and 0.28, while values as low as 0.08 for cold-worked steel (cited for comparison) have been noted [30–32]. The strain-hardening exponent for hot-rolled and annealed Mg alloys varies significantly, depending on the specific alloy composition, processing temperature, and resulting microstructure, but it is generally on the lower end, ranging from 0.08 to 0.21. Factors that influence strain-hardening include the alloy composition, grain size, texture, and even process parameters. For comparison, the strain-hardening exponent cited for annealed AZ31B at 450 °C was

0.16 [30–32]. The strain-hardening exponent was calculated to be an average of 0.13 for as-rolled AXM20504 and 0.21 for AXM20504 for the annealed condition. Thus, the post-annealing did improve the strain-hardening and uniform elongation of the alloy from the as-rolled condition, implying better formability. In previous work regarding AZ31 by Kaseem et al., the calculated strain-hardening exponent (n) increased with increasing rolling temperature, which also explains the corresponding increase in uniform elongation [19].

Post-annealing of the alloys resulted in the increase in the average grain size and the formation of new grain boundary area and, at the same time, it promoted the relieving of internal stresses within the lattice that enabled an increase in ductility, observed for the materials processed by DSR at 20% and 40% reduction, since slip can more readily occur along the newly formed grain boundaries and within a less distorted lattice. The activation of slip in the rolled and post-annealed alloys was evaluated and found to be from the preference of basal and prismatic slip. Schmid's law (also known as the Schmid factor) states that slip begins in a crystalline material when the resolved shear stress on a slip system reaches a critical value, known as the critical resolved shear stress, and indicates that the slip system with the largest Schmid factor will yield first [33,34]. For comparison, the basal and prismatic slip systems were evaluated for the AXM alloys. Based on EBSD data, the average Schmid factor for the single-pass rolled DSR 40% for AXM20504 (prior to annealing) was 0.27 for basal and 0.38 for prismatic, while the average Schmid factor for the post-annealed AXM20504 (average of all post-annealed) was 0.28 for basal and 0.39 for prismatic. The Schmid factors were very similar for the as-rolled and post-annealed alloys—implying the importance of other slip systems like the prismatic orientation, since the Schmid Factor was observed to be higher for both the as-rolled and post-annealed conditions. This also demonstrates that the post-annealed alloys were able to overcome the CRSS of other slip systems like the prismatic slip system to achieve an improvement in ductility.

Another important factor to consider in the static recrystallization process is the Grain orientation spread (GOS), which is a measure of the average misorientation angle between each point within a crystal grain and the grain's average orientation. The GOS is calculated by averaging deviation angles of all pixels within a grain from its mean orientation and this can give clarity to the material's internal state: particularly the degree of plastic deformation and recrystallization [35]. By definition, materials with higher GOS values are often more deformed, while lower GOS values indicate a higher degree of recrystallization. In a GOS map, a color is used to represent each grain. Regions with similar colors have little orientation spread, while areas with significant color changes indicate larger orientation differences. Processed Mg alloys can have a high GOS, with some studies showing a specific peak at 86°. Some recrystallized DRXed grains can have a random texture and an average GOS of less than five, while deformed grains contribute to the basal texture with recrystallized grains (DRX grains) typically having higher GOS values that are greater than five [36]. Annealing will generally decrease GOS by causing recrystallization, where new, strain-free grains form with lower internal misorientation, where the GOS is often defined as less than five [34]. The annealing dissipates the stored strain energy from its prior deformation, reducing the average GOS of the material. The GOS for the as-rolled AXM20504 at DSR 40% was an average of 6.54 ± 3.75, as determined through EBSD data, while the GOS for the AXM20504 post-annealed at 450 °C and 40 min was 0.441 ± 0.401.

The associated GOS maps are shown in Figure 14. The EBSD data reveals that the post-annealing significantly reduced the GOS, confirming the presence of new strain-free grains throughout the microstructure with significantly lower internal misorientation and less lattice distortion.

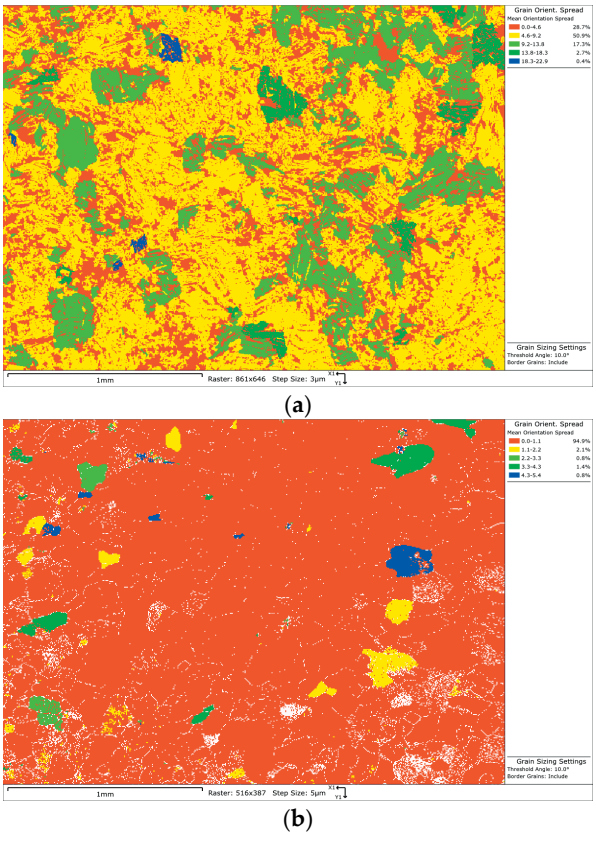


Figure 14. Influence of DSR and post-annealing on the grain orientation spread (GOS) for (**a**) DSR processed at 40% and (**b**) post-annealing at 450 °C for 40 min.

From analysis of the data, including that obtained from EBSD and mechanical testing as well as evaluation through KAM, GOS, and Schmid Factor evaluation, there is a general trend observed in the improvement of ductility through static recrystallization with an increasing temperature from 350 to 400 and 450 °C, due to the relieving of stresses, weakening of the basal texture, and the ability of slip to occur more readily while also maintaining a reasonable tensile strength, relative to the DSR-processed material. Ongoing studies are being performed to use the current rolled and annealed data in the construction of a reliable and predictive model for predicting static recrystallization in these Mg-based alloys.

5. Conclusions

The key outcome from this study was that the strength of Mg-based AXM alloys was enhanced by single-pass DSR through grain refinement via DRX, but the ductility required improvement to enhance the formability. The formability was improved through subsequent post-annealing, resulting in nearly complete recrystallization (SRX). Tensile tests revealed that the ductility was improved from an average of 5% for the DSR processed alloys to nearly 12% for the post-annealed alloys, while the tensile strength was retained above 200 MPa for the post-annealed DSR 40% alloys.

A second key point is that post-annealing effectively relieved the internal stresses that correlated to less lattice distortion and improved ductility, and correspondingly enhanced formability. The lower KAM and GOS observed for the post-annealed alloys demonstrated that the grains became more “strain free,” as compared to the higher values for the highly deformed as-rolled alloys. This supports the ability for slip to occur more readily during plastic deformation, such as tensile testing.

Another key point is that almost complete recrystallization was reached at a temperature of 450 °C for 40 min, as observed in the calculation of % SRX for each tempera-

ture/duration for both 20% and 40% DSR materials. This temperature and duration showed the most improvement in weakening the basal texture intensity to improve ductility from the as-rolled condition. Furthermore, analysis of the pole figures demonstrated a wider spreading of the pole and weakening of the basal texture for the post-annealed alloys, as opposed to the strong basal texture observed for the as-rolled alloys that was more concentrated in the pole figure.

Additional studies are ongoing in the comparison of AXM alloys to other compositions, including the addition of zinc as an alloying element and its influence on both microstructure and mechanical properties, as well as the effect of multi-pass rolling on the material performance in comparison to its single-pass rolling counterpart.

Author Contributions: Conceptualization, Z.X. and C.H.; methodology, C.H., Z.X., P.D. and J.S.; software, C.H., Z.X. and P.D.; validation, C.H., Z.X. and J.S.; formal analysis, C.H. and Z.X.; investigation, C.H., Z.X., S.F. and J.S.; resources, Z.X., C.H. and J.S.; data curation, C.H. and Z.X.; writing—original draft preparation, C.H. and Z.X.; writing—review and editing, C.H. and Z.X.; visualization, C.H. and Z.X.; supervision, Z.X., C.H. and J.S.; project administration, Z.X., C.H. and J.S.; funding acquisition, J.S. and Z.X. All authors have read and agreed to the published version of the manuscript.

Funding: Research funding was provided by NSF Manufacturing: CMMI-2026313; Manufacturing of High Strength, High Ductility, Rare Earth-Free Magnesium Alloy Plate and Sheet Materials by Differential Speed Rolling. Also, funding was partially provided by ERC HAMMER: EEC-2133530; NSF Engineering Research Center for Hybrid Autonomous Manufacturing, Moving from Evolution to Revolution.

Data Availability Statement: The original contributions presented in the study are included in the article. Further inquiries can be directed to the corresponding authors.

Acknowledgments: All the authors would like to thank the entire team at North Carolina A&T State University who supported this research project.

Conflicts of Interest: The authors declare no conflicts of interest.

References

1. Stoudt, M.R. Magnesium: Applications and Advanced Processing in the Automotive Industry. *JOM* **2008**, *60*, 56. [CrossRef]
2. Partridge, P.G. The Crystallography and Deformation Modes of Hexagonal Close-Packed Metals. *Metall. Rev.* **1967**, *118*, 169. [CrossRef]
3. Koike, J.; Kobayashi, T.; Mukai, T.; Watanabe, H.; Suzuki, M.; Maruyama, K.; Higashi, K. The Activity of Non-Basal Slip Systems and Dynamic Recovery at Room Temperature in Fine-Grained AZ31b Magnesium Alloys. *Acta Mater.* **2003**, *51*, 2055–2065. [CrossRef]
4. Ion, S.E.; Humphreys, F.J.; White, S.H. Dynamic Recrystallisation and the Development of Microstructure during the High Temperature Deformation of Magnesium. *Acta Metall.* **1982**, *30*, 1909–1919. [CrossRef]
5. Perez-Prado, M.T.; del Valle, J.A.; Contreras, J.M.; Ruano, O.A. Microstructural evolution during large strain hot rolling of an AM60 Mg alloy. *Scr. Mater.* **2004**, *50*, 661–665. [CrossRef]
6. del Valle, J.A.; Ruano, O.A. Influence of texture on dynamic recrystallization and deformation mechanisms in rolled or ECAPed AZ31 magnesium alloy. *Mater. Sci. Eng. A* **2008**, *487*, 473–480. [CrossRef]
7. Xu, Y.; Hua, L.; Sun, Y. Deformation Behavior and Dynamic Recrystallization of AZ61 Magnesium Alloys. *J. Alloys Compd.* **2013**, *580*, 262–269. [CrossRef]
8. Hale, C.; Xu, Z.; Sankar, J. Optimization of Mechanical Properties in Magnesium-Zinc Alloys. In Proceedings of the TMS 2021, Virtual, 15–18 March 2021; pp. 1–16.
9. Hale, C.; Xu, Z.; Zhang, H.; Yarmolenko, S.; Sankar, J. Comparison of Single-Pass Differential Speed Rolling (DSR) and Conventional Rolling (CR) on the Microstructure and Mechanical Properties of Mg_5Zn. *Curr. Mater. Sci. Former. Recent Pat. Mater. Sci.* **2023**, *16*, 431–442.
10. Jain, J.; Poole, W.J.; Sinclair, C.W. Reducing the Tension-Compression Yield Asymmetry in a Mg-8Al-0.5Zn Alloy via Precipitation. *Scr. Mater.* **2010**, *62*, 301–304. [CrossRef]
11. Li, X.; Yang, P.; Wang, L.-N.; Meng, L.; Cui, F. Orientational Analysis of Static Recrystallization at Compression Twins in a Magnesium Alloy AZ31. *Mater. Sci. Eng. A* **2009**, *517*, 160–169. [CrossRef]

12. Liang, S. Deformation and Its Effect on Recrystallization in Magnesium Alloy AZ31. Master's Thesis, McMaster University, Hamilton, ON, Canada, 2012.
13. Sandlöbes, S.; Friák, M.; Zaefferer, S.; Dick, A.; Yi, S.; Letzig, D.; Pei, Z.; Zhu, L.-F.; Neugebauer, J.; Raabe, D. The Relation Between Ductility and Stacking Fault Energies in Mg and Mg-Y Alloys. *Acta Mater.* **2012**, *60*, 3011–3021. [CrossRef]
14. Stanford, N. The Effect of Rare Earth Elements on the Behavior of Magnesium-Based Alloys: Part 2—Recrystallization and Texture Development. *Mat. Sci. Eng. A* **2013**, *565*, 469–475. [CrossRef]
15. Miura, H.; Ito, M.; Yang, X.; Jonas, J.J. Mechanisms of Grain Refinement in Mg-6Al-1Zn Alloy During Hot Deformation. *Mater. Sci. Eng. A* **2012**, *538*, 63–68. [CrossRef]
16. Levinson, A.; Mishra, R.K.; Doherty, R.D.; Kalidindi, S.R. Influence of Deformation Twinning on Static Annealing of AZ31 Mg Alloy. *Acta Mater.* **2013**, *61*, 5966–5978. [CrossRef]
17. Barnett, M.R. Twinning and the Ductility of Magnesium Alloys. *Mater. Sci. Eng. A* **2007**, *464*, 1–7. [CrossRef]
18. Jain, J. The Deformation Behaviour of a Mg-8Al-0.5Zn Alloy. Ph.D. Thesis, Materials Engineering, The University of British Columbia, Vancouver, BC, Canada, 2010.
19. Kaseem, M.; Chung, B.K.; Yang, H.W.; Hamad, K.; Ko, Y.G. Effect of deformation temperature on microstructure and mechanical properties of AZ31 Mg alloy processed by differential-speed rolling. *J. Mater. Sci. Technol.* **2015**, *31*, 498–503. [CrossRef]
20. Hamad, K.; Ko, Y.G. A cross-shear deformation for optimizing the strength and ductility of AZ31 magnesium alloys. *Sci. Rep.* **2016**, *6*, 29954. [CrossRef]
21. Ko, Y.G.; Hamad, K. Structural features and mechanical properties of AZ31 Mg alloy warm-deformed by differential speed rolling. *J. Alloys Compd.* **2018**, *744*, 96–103. [CrossRef]
22. Hamad, K.; Ko, Y.G. Continuous differential speed rolling for grain refinement of metals: Processing, microstructure, and properties. *Crit. Rev. Solid State Mater. Sci.* **2019**, *44*, 470–525. [CrossRef]
23. Hale, C.; Xu, Z.; Fialkova, S.; Rawles, J.; Sankar, J. Influence of Processing Temperature and Strain Rate on the Microstructure and Mechanical Properties of Magnesium Alloys Processed by Single-Pass Differential Speed Rolling. *Crystals* **2024**, *14*, 262. [CrossRef]
24. Li, Z.T.; Zhang, X.D.; Zheng, M.Y.; Qiao, X.G.; Wu, K.; Xu, C.; Kamado, S. Effect of Ca/Al ratio on microstructures and mechanical properties of Mg-Al-Ca-Mn Alloys. *Mater. Sci. Eng. A* **2017**, *682*, 423–432. [CrossRef]
25. Cao, W.; Chen, S.-L.; Zhang, F.; Wu, K.; Yang, Y.; Chang, Y.; Schmid-Fetzer, R.; Oates, W. PANDAT software with Pan-Engine, Pan-Optimizer and Pan-Precipitation for multi-component phase diagram calculation and materials property simulation. *Calphad* **2009**, *33*, 328–342. [CrossRef]
26. Hale, C. Effect of Differential Speed Rolling on the Dynamic Recrystallization of Lightweight Magnesium Alloys Unver Different Temperatures and Strain Rates. Ph.D. Thesis, North Carolina A&T State University, Greensboro, NC, USA, 2023.
27. *E8/E8M*; Standard Testing Methods for Tension Testing of Metallic Materials. ASTM International: West Conshohocken, PA, USA, 2022.
28. Zhang, H.; Xu, Z.; Yarmolenko, S.; Kecskes, L.; Sankar, J. Evolution of microstructure and mechanical properties of Mg-6Al alloy processed by differential speed rolling upon post-annealing treatment. *Metals* **2021**, *11*, 926. [CrossRef]
29. Huang, X.; Xin, Y.; Cao, Y.; Wei, L.; Huang, G.; Zhao, X.; Liu, Q.; Wu, P. Understanding the mechanisms of texture evolution in an Mg-2Zn-1Ca alloy during cold rolling and annealing. *Int. J. Plast.* **2022**, *158*, 103412. [CrossRef]
30. Hollomon, J.H. Tensile Deformation. *AIME* **1945**, *162*, 268–290.
31. Callister, W.D., Jr. *Fundamentals of Materials Science and Engineering*, 2nd ed.; John Wiley & Sons: Hoboken, NJ, USA, 2005; p. 199.
32. Kalpakjian, S. *Manufacturing Engineering and Technology*, 2nd ed.; Pearson Education South Asia Pte: Singapore, 2014; p. 62.
33. Roll Formed Aluminum Alloy Components, *ASM Handbook*, 10th ed.; Handbook Committee; ASM International: Materials Park, OH, USA, 2005; p. 482.
34. Rollett, A.D. Plastic Deformation of Single Crystals. In *Texture, Microstructure & Anisotropy Course Notes*; Carnegie Mellon University: Pittsburgh, PA, USA, 2014.
35. Schmid, E.; Boas, W. *Kristallplastizitat: Mit Besonderer Berucksightigung der Metalle*, 1st ed.; Springer: Berlin/Heidelberg, Germany, 1935; ISBN 978-3662342619. (In German)
36. Hadadzadeh, A.; Mokdad, F.; Wells, M.A.; Chen, D.L. A new grain orientation approach to analyze the dynamic recrystallization behavior of a cast-homogenized Mg-Zn-Zr alloy using electron backscattered diffraction. *Mater. Sci. Eng. A* **2018**, *709*, 285–289. [CrossRef]

Disclaimer/Publisher's Note: The statements, opinions and data contained in all publications are solely those of the individual author(s) and contributor(s) and not of MDPI and/or the editor(s). MDPI and/or the editor(s) disclaim responsibility for any injury to people or property resulting from any ideas, methods, instructions or products referred to in the content.